NSF GRANT # CMMI-1030786
NSF PROGRAM NAME: MME

High Precision Scribing of Thin Film Solar Cells by a Picosecond Laser

P.I.: Yung C. Shin
Purdue University

Gary Cheng (co-PI), Wenqian Hu, Martin Yi Zhang, Seunghyun Lee
Purdue University

Abstract: In this paper, the feasibility of thin-film solar cells scribing via a picosecond (ps) laser is investigated. The optical and thermal properties of thin films are studied first. Next, molybdenum and ZnO thin films are deposited on soda lime glass substrates by pulsed laser deposition. Then experiments for picosecond laser scribing are performed with different wavelengths and average powers and results are analyzed for process parameter optimization. The scribed slots are measured using a surface profilometer and a scanning electron microscope (SEM). Using the optimized laser parameters, the ablation depths of the slots are accurate within 0.1 μm tolerance, the edges are sharp without distortions and slot bottoms are flat. These slots are precisely machined with a high speed, which makes ps laser scribing of solar cells a promising technique.

1. Introduction: Solar cells have been developed and used as a clean energy source for a long time. The production cost and photovoltaic energy conversion efficiency are two major issues that need to be considered in the design and fabrication process of solar cells. The production cost is greatly reduced in thin-film based solar cells fabrication, as compared to wafer-based solar cells.[1] The energy conversion efficiency of the solar cell is significantly affected by the machining precision of slot geometry, i.e., the edge and the bottom.

For thin-film solar cells, laser scribing has been investigated extensively.[2,3] However, very few high quality slots with sharp edges and flat bottoms have been demonstrated yet. Ps laser has been shown to have the capability of micromachining with high speed and high precision for other applications.[4] If ps laser can also be used for solar cell fabrication, the production cost will be reduced and the performance of the solar cell will be improved. Therefore, high precision solar cell scribing using ps laser ablation is investigated and presented in this paper.

2. Experimental setup: The laser system used in this study consists of a ps Lumera laser (RAPID), a high precision three-axis Aerotech positioning system (ATS125), and a high-speed ScanLab scanner (hurrySCAN 10). This ps laser has an average power of 2 W, a pulse width of 10 ps, and repetition rates in the range from 10 kHz to 500 kHz. The pulse energy can go up to 30 μJ and the peak power is up to 3 MW. The fundamental wavelength (1064 nm) and the second harmonic wavelength (532 nm) are used to perform laser material processing. The three-axis positioning system, with vertical resolution down to 10 nm, is commensurate with the capabilities of the laser and the scanner. It provides vertical (z) movement of the workpiece during micromachining so that the focal spot is maintained at the prescribed position as well as horizontal plane (xy) movement for machining of a larger part, as the ablation is progressing. The scanner is used to ensure the accurate positioning and fast movement of the laser beam over the target. An optical surface profilometer (ADE MicroXAM) and a scanning electron microscope (JOEL 330) are used to measure three-dimensional profiles of the sample.

3. Materials and properties: The thin-film solar cell sample used in this study consists of an absorbent layer (copper indium selenide, CIS), a back contact layer (molybdenum, Mo), and a glass substrate (Fig. 1). A portion of the sample (region II) only has the Mo layer on the glass, so that the machining of Mo can be studied alone without the interference of a CIS layer on top of it. The thicknesses of the CIS layer and the Mo layer are 1.0 μm and 0.5 μm, respectively.

The thermal and optical properties of CIS and Mo are listed in Table 1. CIS is a semiconductor material with a low band gap which is lower than the photon energy at either 532 nm or 1064 nm. Mo is a metal without band gap. Comparing the thermal properties between CIS and Mo, it is easy to see the thermal conductivity, the thermal diffusion length (calculated

at laser pulse duration of 10 ps), and the melting temperature of CIS are much lower than those of Mo. Mo has similar reflectivities at 532 nm and 1064 nm, but the optical penetration depth is smaller at 532 nm. These properties are helpful in investigating how to precisely remove the desired depth of the material without damaging the material below. For example, a high average power (e.g. 100 mW) should not be applied when only the CIS layer needs to be removed, otherwise the Mo layer underneath will be damaged. This conclusion can be verified by the experiments.

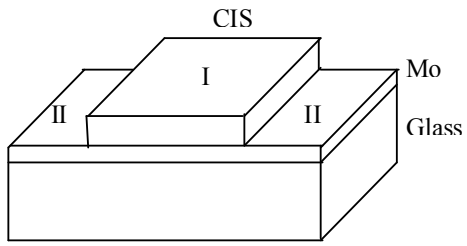

Figure 1: Schematic of the sample

Table 1. Thermal and optical properties of CIS and Mo [5,6]

	CIS	Mo
Band gap E_g (eV)	≈ 1	0
Density ρ (10^3 kg/m^3)	5.77	10.2
Thermal conductivity k_{th} (W/mK)	37	138
Specific heat C_p (10^2 J/kgK)	3	2.5
Thermal diffusion length δ_{th} (nm)	10	50
Melting temperature T_m (K)	1600	2896
Surface reflectivity (at 532 nm/1064 nm)	NA	0.58/0.67
Optical penetration depth (nm) (at 532 nm/1064 nm)	NA	12/35

4. Fabrication Process of the CIGS Thin Film Solar Cell: Solar cells fabricated in this research follow the fabrication process shown in Figure 2. The purchased soda lime glass (diameter of 2" with thickness of 0.04") is ultrasonicately cleaned by acetone, methanol and DI water for 5 minutes, sequentially. The Mo coated soda lime glass substrates used in this study is a 500 nm thick layer fabricated by 200 W dc-magnetron sputtering at Ar gas pressure of 2-10 mTorr [7]. During the deposition, the sample is rotated at 5 RPM. The deposition time is 20 minutes. After deposition of Mo, the CIGS nanocrystal precursor layer is deposited on top of the Mo-coated substrates by nanoink precursor printing. The nanoink precursor is bought from commercial suppliers. The sample was then let dry in the air. After the solvents evaporated, a subsequent thermal annealing under Ar gas atmosphere at 400 ^{o}C for 1 hour was performed to remove the organics [8]. The rapid thermal annealing (RTA) method is used to minimize the defects in the absorber layer.

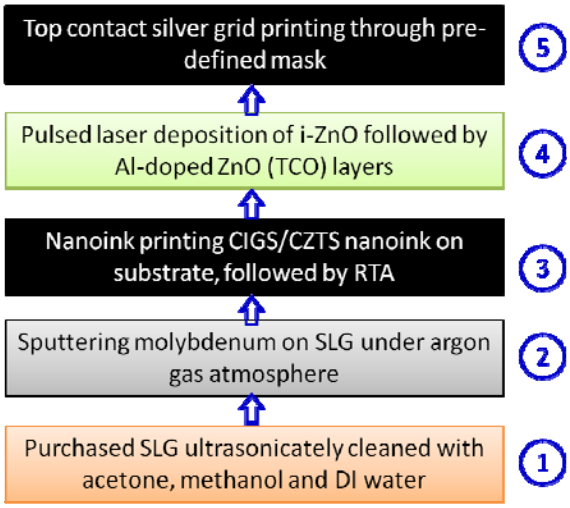

Figure 2: Fabrication process of solar cells.

After RTA, a thin (~50 nm) high resistivity i-ZnO film (window layer) capped with a ~250 nm high conductivity alumina-doped ZnO film (TCO layer) is deposited by pulsed laser deposition [9,10]. Pulsed laser deposition is performed with KrF excimer laser with wavelength of 248 nm, pulsed duration of 25 ns, and repetition rate of 10 Hz. In the PLD vacuum chamber, the target-sample distance is fixed at 80 mm. Oxygen gas is purged to reach the deposition pressure of 150 mTorr. The i-ZnO film is deposited with a pure ZnO (99.99%) target under the laser fluence of 0.5 J/cm^2 for 30 minutes. The TCO layer is deposited with 2% (w.t.%) alumina-doped ZnO (99.99%) target at the laser fluence of 1.5 J/cm^2 for 100 minutes. Both i-ZnO and TCO layer are deposited at room temperature. After deposition of the oxide layers, a silver grid is fabricated on top of the window layer to form the top contact. Noting that all fabrication processes (except for RTA) are performed at room temperature, it makes this method promising to fabricate flexible solar cells that use low melting point materials (e.g. paper and plastics) as a substrate if an alternative low temperature method to replace RTA could be found.

Properties of Deposited Layers

Sputtered Molybdenum 500-nm-thick molybdenum sputtered at room temperature has low resistivity with

average of ~13.7 μΩcm; this is roughly 2.5 times of the bulk Mo value (5.4 μΩcm) at room temperature. The molybdenum film also has good adhesion, which is verified by scotch tape testing. The thickness of Mo film is determined by field emission scanning electron microscope (FESEM) at the cross section of the film, as shown in Figure (a, b). An optical graph of a typical molybdenum film deposited on the 2" round soda lime glass is shown in Figure 3(c), which shows a mirror-like highly reflective surface. The x-ray diffraction (XRD) spectrum gives a sharp peak around 40.5°, which corresponds to (110) diffraction orientation of molybdenum (PDF # 04-0809).

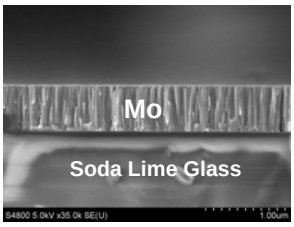

(a) Uniform Mo film at 35 K magnification

(c) Optical graph of sputtered Mo film

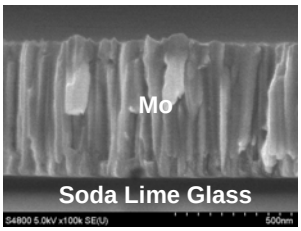

(b) Uniform Mo film at 100 K magnification

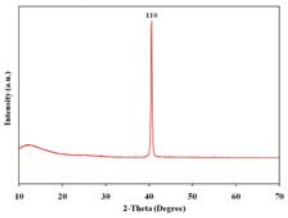

(d) XRD spectrum shows mainly 110 peak

Figure 3: Sputtered 500-nm-thick molybdenum and its properties.

i-ZnO film by Pulsed Laser Deposition Instead of depositing i-ZnO on an absorber layer, trial runs on soda lime glass were carried out here in order to find appropriate deposition parameters. The i-ZnO film prepared by room temperature pulsed laser deposition (PLD) shows promising electrical, optical and structural properties. Top morphology and cross-sectional morphology FESEM images of i-ZnO film are shown in Figure 4. The lower resolution top morphological FESEM image shows: (a) the deposited film is pretty uniform as expected, while the higher resolution one and (b) the particle size is in the range of 25 - 40 nm. Cross sectional FESEM images (c, d) show the thickness is around 50 nm. Since the deposition time is 30 minutes, the deposition rate could be determined to be 1.67 nm/minute. The deposition rate could be used as reference as an i-ZnO film is deposited on a CIGS absorber layer in future experiments.

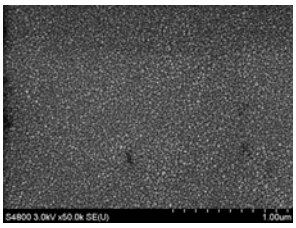

(a) Top morphological at 50 K

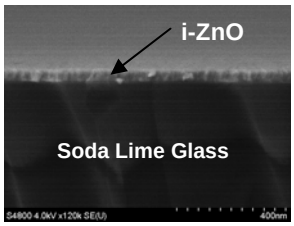

(c) Cross sectional morphological at 120 K

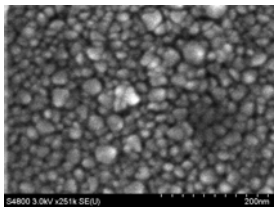

(b) Top morphological at 251 K

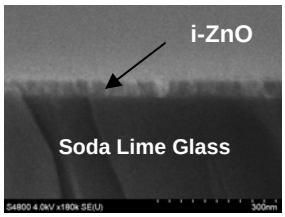

(d) Cross sectional morphological at 300 K

Figure 4: Top (a, b) and cross-sectional (c, d) FESEM micrographs of PLD i-ZnO.

Structural analysis is performed by X-ray diffraction. Figure 5 shows the XRD spectra of i-ZnO film grown via room temperature PLD. Compare to the spectrum of SLG substrate, a sharp peak at around 34.3°, which corresponds to (002) diffraction orientation of crystalline ZnO (PDF # 05-0664), is found in the spectrum. This exhibits a high c-axis orientation with wurtzite structure [11]. The full width at half maximum (FWHM) of the (002) peak is measured to determine the particle size (D) as it could be calculated from Scherrer formula: $D = 0.9\lambda/\beta\cos\theta$ [12], where λ is the radiation wavelength (1.5418 Å for Cu *Ka* in this case), β is the FWHM value measured from XRD spectrum, and θ is the Bragg angle of (002) peak which could be obtained from XRD spectrum. The D value is calculated to be 35 nm for i-ZnO, which agrees well with what is observed from FESEM characterization.

The optical transmission spectrum is also measured by UV-vis-NIR spectrometry, Figure 6(a). The visible transmittance ranges from 87.3% to 91% with an average of 89%. The near-infrared (NIR) transmittance ranges from 86.3% to 90.6% with an average value of 88%. The absorption edge could also be observed in the UV region, where the optical bandgap energy (E_g) of the *i*-ZnO film could be evaluated from the Tauc relation [13] and plotted in Figure 6(b). The E_g is determined to be 3.34 eV, which is close to the bandgap of ZnO, 3.3 eV. The

small deviation of the bandgap energy is attributed to the Burstein-Moss effect, polaron, strain, and some other types of imperfections of the film [11].

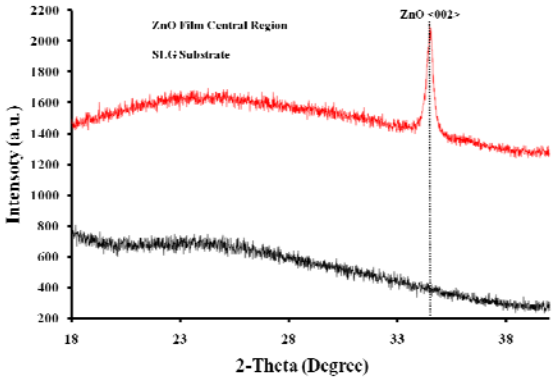

Figure 5: XRD spectra of i-ZnO on SLG substrate (red) and SLG substrate itself (black).

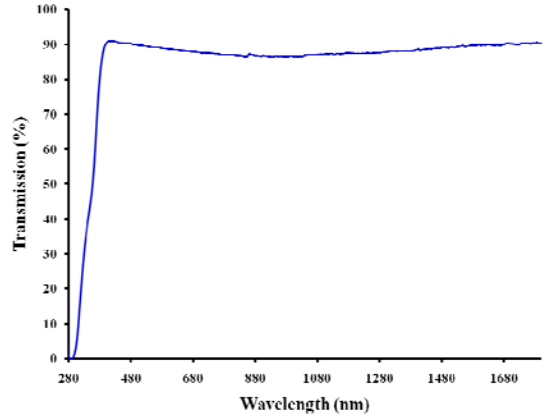

(a) Optical transmission spectrum of ZnO film deposited at room temperature

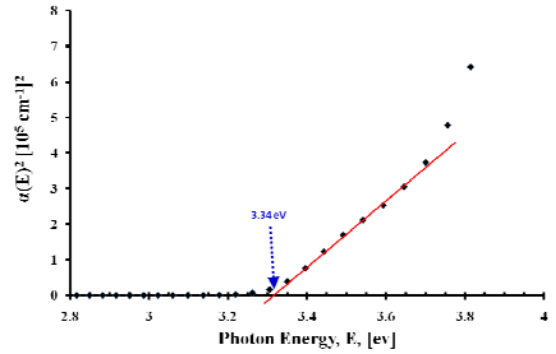

(b) Bandgap energy (E_g) ZnO film deposited at room temperature

Figure 6: Optical transmission spectrum and corresponding Bandgap energy of i-ZnO film deposited at room temperature via pulsed laser deposition.

5. **Experiments and results:** Several series of experiments were done to investigate the appropriate laser parameters to ensure that a desired depth of the material is removed without damaging the material below. The first series of experiments was performed at 532 nm. Different average powers (20 mW to 80 mW) and numbers of scans (1 to 20) were applied to machining region I of the sample (see Fig. 1) with two layers CIS and Mo, at repetition rate of 10 kHz and a scanning speed of 0.12 m/s. Although the processing parameters were different, the ablation depths were all about the thickness of the CIS layer (1 μm) and protrusions occurred on the material due to the melting of the Mo layer. For example, two slots machined with 63.0 mW average power and different scans are shown in Fig. 7. For these two slots, the machined slot zone both protrudes out of the surface with the slot edge 1 μm higher than the unmachined surface. As the scan number is increased from 1 to 20, only the slot width increases (30 μm to 70 μm) but the ablation depth maintains at 1 μm. This phenomenon could happen if a significant amount of photons transmit through the thin CIS layer before CIS is removed, but the transmitted photons would just melt the Mo layer instead of ablating. After the CIS layer is removed, the surface protrusion has occurred, so it will be more likely that the photons were reflected away from the convex surface than to ablate the Mo layer. Therefore, the results were not satisfactory and 1064 nm (i.e., smaller photon energy) was used for the second series of experiments. It was found that the machining of CIS with a high average power (100 mW to140 mW) at 1064 nm yielded similar protrusions of 1 μm as at 532 nm, which matched with the conclusion in the last section. The machining of Mo at a high average power (100 mW to140 mW) was not good either since the glass substrate was damaged, as shown in Fig. 8. In the third series of experiments, lower average powers and lower laser spot overlapping ratios were applied. It was found that the average power around 50 mW was good for machining of Mo as long as the overlapping ratio is higher than 75%. To machine the CIS layer alone, a low power around 20 mW should be used.

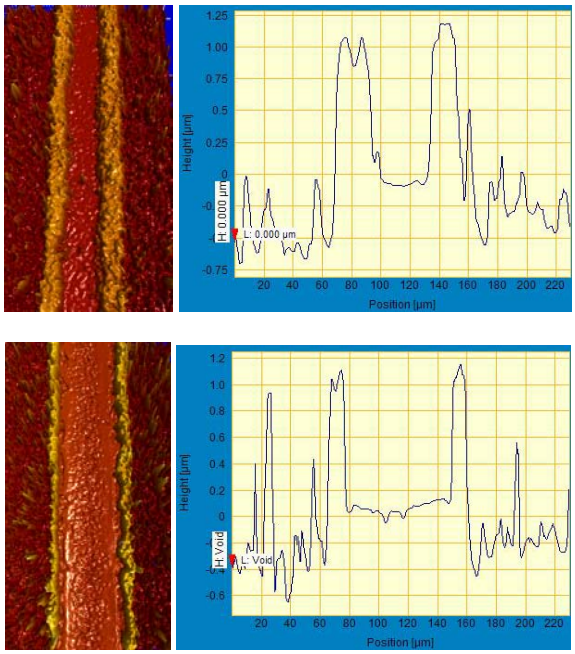

Figure 7: Three-dimensional and two-dimensional profiles of two slots machined on CIS. Laser wavelength: 532 nm; average power: 63.0 mW; number of scans: 1/20 (top/bottom).

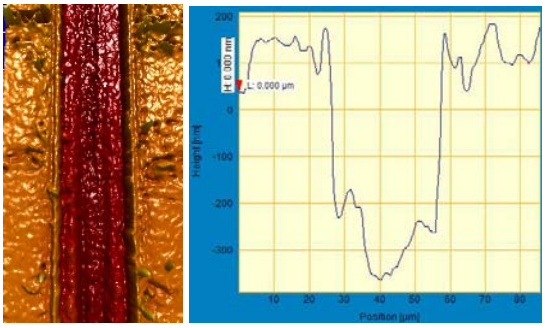

Figure 8: Three-dimensional and two-dimensional profiles of a slot machined on Mo. Laser wavelength: 1064 nm; average power: 100.8 mW; number of scans: 5.

The optimal parameters for machining Mo, CIS, CIS/Mo are shown in Table 2. It should be noted that the laser spot overlapping ratio in Table 2 is a number for reference only, because the actual ablation spot sizes on CIS and Mo are a little different. This overlapping ratio also depends on the laser repetition rate and scanning speed.

Table 2. Laser processing parameters

	Mo	CIS	CIS/Mo
Laser repetition rate	10 kHz		
Laser average power	50.1 mW	21.0 mW	39.3 mW
Laser wavelength	1064 nm		
Laser spot size	30 µm for CIS and 20 µm for Mo		
Laser spot overlapping ratio	75%	93.75%	93.75%
Laser scanning speed	0.04 m/s	0.01 m/s	0.01 m/s
Number of scans	5	1	4

The machined slots were measured by the surface profilometer and the SEM, as shown in Figs. 9-11. The SEM images in Figs. 9-11 were obtained with the sample tilted at 30º and a magnification of 2000 times. Fig. 9 shows a slot scribed on the Mo layer, which is straight with sharp edge and flat bottom. The depth of this slot is 0.468 (≈ 0.5) µm. The profiles of a slot on the CIS layer are shown in Fig. 10. The CIS layer of the sample has a large surface roughness before machining, and the unevenness of the surface is not caused by the machining process. It can be seen that the bottom of the slot on the CIS layer is smoother than the pre-machined CIS surface. The slot shown in Fig. 11 is cut through the Mo and the CIS layers and also has high precision. The depth of this slot is 2.04 (≈ 2) µm, which is the total thickness of the Mo and the CIS layers. The slot widths in the CIS and the Mo layer are 30 µm and 20 µm, respectively, so a stepped profile appears at the interface of the CIS layer and the Mo layer. The ablation threshold of Mo is higher than that of CIS, so the slot width is narrower due to the spatial Gaussian laser pulse tail effect.

6. Conclusion: In this report, a preliminary result of solar cell thin film scribing by a picosecond laser system has been presented. Thin molybdenum and ZnO films were successfully deposited on soda lime glass substrates first by pulsed laser deposition. High precision slots were obtained with sharp edges and flat bottoms. The ablation depth of the slot was precisely controlled so that the exact thickness of a material layer can be removed without damaging the material beneath. This is due to the short pulse duration of the ps laser and appropriate laser average powers. Moreover, the slots were machined with a high scanning speed, which makes ps laser scribing of solar cells practical for industries.

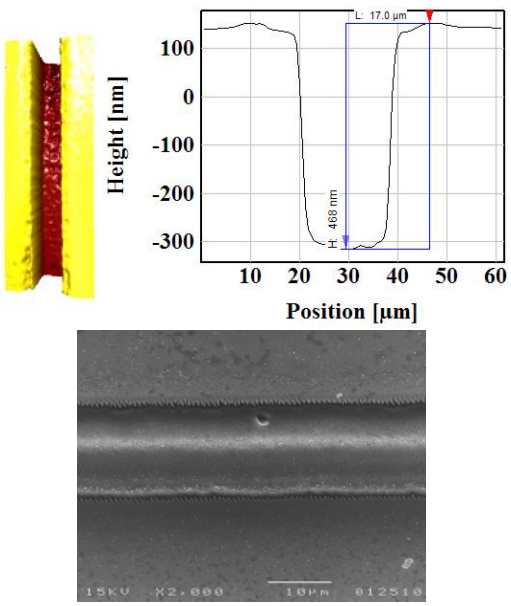

Figure 9: Three-dimensional, two-dimensional profiles and the corresponding SEM image of a slot machined on Mo

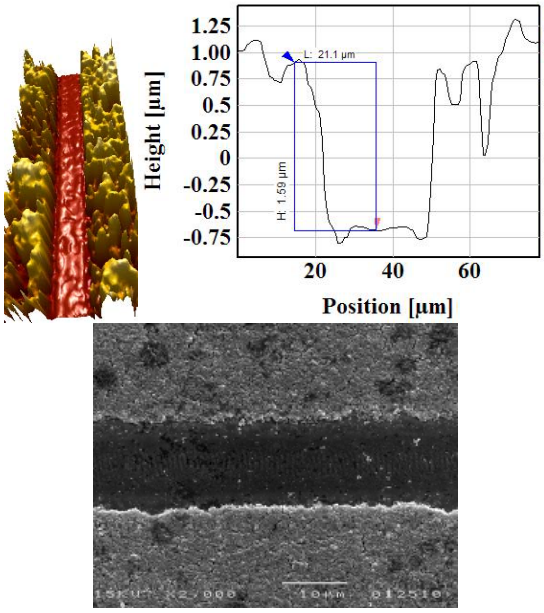

Figure 10: Three-dimensional, two-dimensional profiles and the corresponding SEM image of a slot machined on CIS

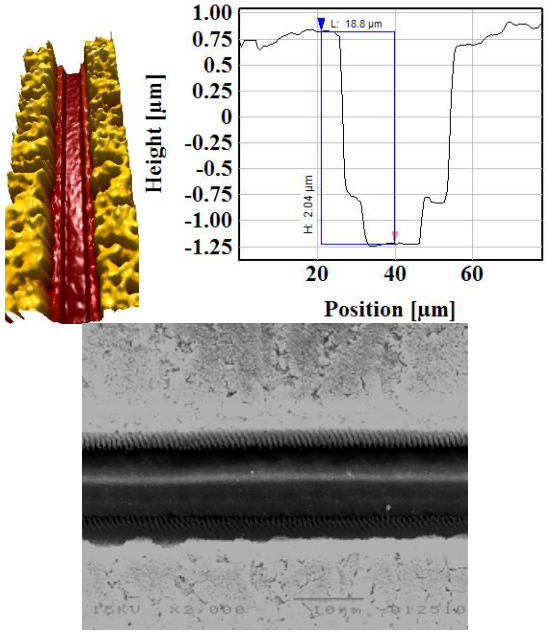

Figure 11: Three-dimensional, two-dimensional profiles and the corresponding SEM image of a slot machined through CIS/Mo

7. Acknowledgement: The authors wish to gratefully acknowledge the financial support provided for this study by the National Science Foundation (Grant No: CMMI-1030786).

8. References:

[1] Y. Hamakawa (Ed.), *Thin-film solar cells: next generation photovoltaics and its applications*, Springer-Verlag, Berlin Heidelberg (2004).

[2] H.P. Huber, F. Herrnberger, S. Kery, and S. Zoppel, Selective structuring of thin-film solar cells by ultrafast laser ablation, *SPIE* **6881**, 688117 (2008).

[3] J. Hermann, M. Benfarah, S. Bruneau, E. Axente, G. Coustillier, T. Itina, J.F. Guillemoles, and P. Alloncle, Comparative investigation of solar cell thin film processing using nanosecond and femtosecond lasers, *J. Phys. D: Appl. Phys.* **39**, 453 (2006).

[4] W. Hu, Y.C. Shin, and G.B. King, Micromachining of metals, alloys, and ceramics by picosecond laser ablation, *Trans. of the ASME J. Manuf. Sci. Eng.* **132**, 011009 (2010).

[5] D.R. Lide (Ed.), *Handbook of Chemistry and Physics* 73th edition, CRC Press (1993)

[6] E.D. Palik (Ed.), *Handbook of Optical Constants of Solids*, Elsevier (1998).

[7] J.H. Scofield, A. Duda, D. Albin, B.L. Ballard, P.K. Predecki, Sputtered molybdenum bilayer back contact for copper indium diselenide-based polycrystalline thin-film solar cells, *Thin Solid Films*, 260, pp 26-31, 1995.
[8] Q. Guo, S.J. Kim, M. Kar, W.N. Shafarman, R.W. Birkmire, E.A. Stach, R Agrawal, H.W. Hillhouse, Development of CuInSe2 nanocrystal and nanoring inks for low-cost solar cells, *Nano Lett.*, vol 8, no. 9, 2982-2987, 2008.
[9] Y. Nakata, T. Okada, M. Maeda, Deposition of ZnO film by pulsed laser deposition at room temperature, *Appl. Surf. Sci*., 197-198, 368-370, 2002.
[10] K. Matsubara, P. Fons, K. Iwata, A. Yamada, S. Niki, Room-temperature deposition of Al-doped ZnO films by oxygen radical-assisted pulsed laser deposition, *Thin Solid Films*, 422, 176-179, 2002.
[11] X. Ma, J. Zhang, J. Lu, Z. Ye, Room temperature growth and properties of ZnO films by pulsed laser deposition, *Appl. Surf. Sci*., 254, 1310-1313, 2010.
[12] A.L. Patterson, The Scherrer Formula for X-ray particle Size Determination, *Phys. Rev*. 56, 978-982, 1939.
[13] J. Tauc, R. Grigorovici, A. Vancu, Optical properties and electronic structure of amorphous germanium, *Phys. Stat. Sol*., 15, 1966, 627.